



CHORUS

This is the accepted manuscript made available via CHORUS. The article has been published as:

Formation of a Novel Ordered Ni₃Al Surface Structure by Codeposition on NiAl(110)

Yong Han, Barış Ünal, and J. W. Evans

Phys. Rev. Lett. **108**, 216102 — Published 23 May 2012

DOI: [10.1103/PhysRevLett.108.216102](https://doi.org/10.1103/PhysRevLett.108.216102)

Formation of a novel Ordered Ni₃Al Surface Structure by Codeposition on NiAl(110)

Yong Han,^{1,*} Barış Ünal,^{2,3} and J. W. Evans^{3,4}

¹*Institute for Physical Research and Technology, Iowa State University, Ames, IA 50011*

²*Department of Chemical Engineering, Massachusetts Institute of Technology, Cambridge, MA 02139*

³*Ames Laboratory-USDOE, Iowa State University, Ames, IA 50011*

⁴*Department of Physics and Astronomy, Iowa State University, Ames, IA 50011*

Formation of a new type of ordered 2D Ni₃Al overlayer by low-temperature codeposition on NiAl(110) is demonstrated by KMC simulation of a multisite atomistic lattice-gas model with a precise treatment of surface diffusion kinetics. Simultaneous codeposition with 3:1 Ni:Al yields poor ordering at 300 K, but well-ordered structures by ~ 500 K. Sequential codeposition of Ni then Al yields unmixed core-ring nanostructures at 300 K, but strong intermixing and ordering by ~ 500 K.

PACS numbers: 68.35.bd, 68.55.A-, 68.35.Md, 68.55.J-

Intermetallics based on Ni aluminides have been studied extensively for structural applications due to their wear, oxidation, and corrosion resistance [1, 2]. Such alloys are also used in steam reforming, Ni₃Al in particular resisting carburization and metal dusting [3], and for broader catalysis applications [4]. Intensive recent activity has involved the use of Ni aluminides as substrates for ultrathin oxide films [5, 6] which support transition metal nanoclusters constituting model catalyst systems [7, 8], and also direct assembly of arrays of magnetic metal nanoclusters for spintronics applications [9]. The structure and properties of the ultrathin oxide surface are impacted by the underlying substrates. All these examples motivate our theoretical exploration of novel routes for fabrication of modified types of Ni aluminide surfaces with refined surface properties compared to bulk terminations of NiAl and Ni₃Al.

As background to our study, we note that Ni-Al films have been created previously by deposition or codeposition procedures followed by annealing. Deposition of Al on Ni(111) produces various ordered compositions after annealing to ~ 780 K [10]. Other studies deposited Ni on Al(111) [11]. Sequential codeposition of alternating layers of Ni and Al forms an intermixed alloy at higher temperatures (T) [12] or after applying a reaction trigger [13]. Our approach also involves codeposition of Ni and Al, but contrasting previous studies: (i) dynamics is constrained to a single layer avoiding intermixing with the substrate; (ii) a realistic atomistic-level model is developed elucidating the complex kinetics of alloy ordering. Thus, our work also connects with broad interest in elucidating not just equilibria but kinetics of metallic surface alloys [14, 15].

Our specific goal is to demonstrate the viability of synthesizing a new type of Ni₃Al surface structure by low- T codeposition of Ni and Al on NiAl(110). The NiAl(110) surface has 1:1 Ni:Al stoichiometry with rectangular unit cell dimensions $a_x = 0.4083$ nm in the $[\bar{1}10]$ x -direction, and $a_y = 0.2887$ nm in the $[001]$ y -direction (in our schematics). Our new Ni₃Al structure with a $a_x \times 2a_y$ unit cell is shown in Fig. 1(a). This structure is dis-

tinct from all surface structures of bulk Ni₃Al, including the (111) surface with 3:1 Ni:Al composition [16]. See Fig. 1(b). Our density functional theory (DFT) analysis (details in [17, 18]) analysis shows that the distinct geometric structure implies distinct electronic and related properties, but here we focus on formation kinetics.

Success of our codeposition approach requires the existence of a low- T far-from-equilibrium formation pathway to avoid intermixing. DFT analysis finds a high 1.14 eV barrier for thermodynamically unfavorable exchange of a Ni adatom with surface Al, and barriers for other exchange processes are higher. Thus, intermixing processes are too slow to occur on the short time-scale of diffusion-mediated incorporation of deposited atoms into surface nanostructures at 300–600 K (incorporation locks adatoms in the overlayer). The situation is different from Ni deposition on Al, or Al on Ni, where there is a strong driving force for intermixing. Another feature implying a 2D growth mode is that no strong thermodynamic driving force for multilayer growth, but strong kinetic inhibition to upward transport and higher-layer nucleation at lower T and low coverages. (DFT finds an energy per Ni₃Al unit in the monolayer structure of Fig. 1(b) only marginally higher by 0.11, 0.17, ... eV than in the analogous bilayer, trilayer, ... structures).

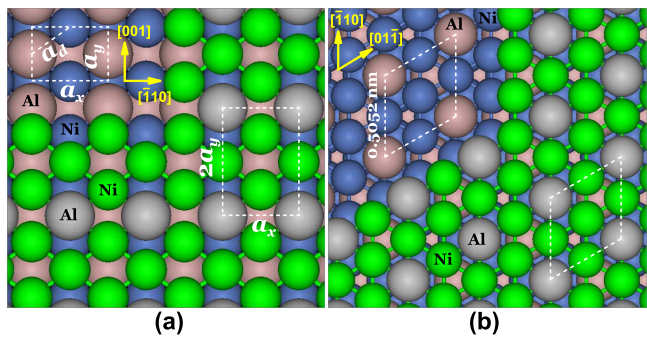


FIG. 1. (a) Ni₃Al/NiAl(110); (b) Ni₃Al(111). Structure of underlying layers is indicated upper left. Top (lower) layer Ni is green (blue); top (lower) layer Al is grey (purple).

For realistic atomistic-level modeling of the far-from-equilibrium formation of 2D Ni₃Al alloy nanostructures, it is essential to describe not just the surface thermodynamics (e.g., the relative energies of various 2D structures), but also the surface diffusion kinetics. In addition to accurately describing the adsorption site energies and diffusion of isolated Ni and Al adatoms, the major challenge is to also precisely describe edge diffusion, rearrangement, and attachment-detachment processes for vast numbers of local step-edge configurations and compositions occurring in irregular multi-component surface nanostructures. Growth structures are extremely sensitive to the associated hopping barriers [19].

To successfully address this challenge, we exploit a recently developed multisite lattice-gas model formulation which can describe multiple adsorption sites and diffusion paths with precise hopping barriers [17, 18]. We now briefly describe this model and its validation. We allow occupation of two types of stable adsorption site, Ni-br (and Al-br) denoting the short-bridge between two surface Ni (and Al) atoms separated in the y -direction by a_y . Fig. 2(a) shows both DFT adsorption energies and diffusion paths and barriers for isolated Ni and Al adatoms. Both prefer the Ni-br site, even though Ni resides at the Al-br site in an equilibrated NiAl alloy overlayer.

Adlayer thermodynamics is determined by adsorption energies and by interactions between adatoms at Ni-br and Al-br sites. DFT-guided estimates for Al-Al and Ni-Ni (Ni-Al) pair interactions are shown in Fig. 2(b) (Fig. 2(c)). There are 16 such significant interactions. Many-body interactions are not substantial. See below. When adatoms aggregate, there is a preference for “dense” islands with both Al-br and Ni-br sites populated, the cost of populating less favorable Al-br sites being offset by strong diagonal attractions for separation $a_d = 0.2500$ nm.

Model thermodynamics is validated by comparing energies from direct DFT analysis of complete overlayers with predictions from our pairwise interaction model for: (i) dense single-species islands versus “dilute” islands with adatoms on just Ni-br or just Al-br sites; (ii) perfectly ordered alloy overlayer propagating bulk structure versus one with Ni and Al on the wrong sites (Ni on Ni-br, Al on Al-br), versus “phase-separated” dense Ni and Al domains. The model predicts the correct ordering of energies (i.e., the correct relative stability) [18, 20].

Next, we describe the model treatment of diffusion kinetics. Ni always makes diagonal hops. Al diffusion along island edges can occur as for isolated Al or by diagonal hops. See Figs. 2(a)-2(h). Hopping barriers are determined as $E_{\text{act}} = E_{\text{TS}} - E_{\text{init}}$, where $E_{\text{init}}(E_{\text{TS}})$ is the total energy in the initial (transition) state. Both energies are obtained from a sum of the relevant adsorption energy and all pair interaction energies. Thus, in addition to conventional pair interactions between adatoms both at adsorption sites, we must also assess a sec-

TABLE I. Pair interactions in eV: one adatom at a Al-br or Ni-br site, and one at a t or b TS. See Fig. 2(d).

Ni(b)-Ni(1)	-0.30	Al(b)-Al(1)	-0.45	Al(t)-Al(4)	-0.02
Ni(b)-Ni(2)	-0.14	Al(b)-Al(2)	-0.40	Al(t)-Al(5)	+1.00
Ni(b)-Ni(3)	-0.18	Al(b)-Al(3)	-0.20	Al(t)-Al(6)	+12.00
Ni(b)-Ni(4)	-0.25	Al(b)-Al(4)	-0.29	Al(t)-Al(7)	-0.12
Ni(b)-Al(1)	-0.85	Al(b)-Ni(1)	-0.73	Al(t)-Ni(4)	-0.01
Ni(b)-Al(2)	-0.28	Al(b)-Ni(2)	-0.24	Al(t)-Ni(5)	-0.44
Ni(b)-Al(3)	-0.14	Al(b)-Ni(3)	-0.18	Al(t)-Ni(6)	+6.50
Ni(b)-Al(4)	-0.71	Al(b)-Ni(4)	-0.62	Al(t)-Ni(7)	-0.06

ond set of “unconventional” pair interactions with one adatom at a TS and another at nearby adsorption site. There are 24 such significant interactions: Al(t)-M(4-7), Al(b)-M(1-4), Ni(b)-M(1-4), with M=Al or Ni. See Fig. 2(d) and Table I. Adatom hopping occurs with Arrhenius rates $h = \nu \exp[-E_{\text{act}}/(k_B T)]$ for prefactor $\nu = 10^{-13}$ /s. Detailed-balance is automatically satisfied. Kinetic Monte Carlo (KMC) simulation of the model simply implements deposition and hopping with probabilities proportional to the relevant rates.

To validate model kinetics, we have checked that the model recovers STM observations of: (i) transitions with varying T between various complex growth shapes of Ni islands for Ni deposition on NiAl(110) [20]; (ii) the change with increasing size from compact to irregular growth shapes of Al islands formed by Al deposition at 300 K [18]; (iii) robust Al-core plus Ni-ring nanostructures obtained by sequential deposition of Al then Ni at 300 K [17]. Distinct behavior for deposition of Ni then Al at 300 K is also recovered (see below).

Thermodynamics for 3:1 Ni:Al compositions.

First, we determine the preferred adlayer ordering for our model for complete overlayers with 3:1 Ni:Al stoichiometry and where Ni and Al adatoms occur with just a few distinct types of local configurations. For each such configuration, we calculate the adatom energy by summing the adsorption energy and half the shared lateral pairwise interactions, and then average over configurations to obtain the mean energy per Ni atom, E_{Ni} , and per Al atom, E_{Al} . Finally, the overlayer energies, $E_{3\text{Ni}+\text{Al}} = 3E_{\text{Ni}} + E_{\text{Al}}$, are compared for: (I) “perfect” Ni₃Al ordering with Ni on all Al-br sites, and alternating Ni and Al in vertical rows of Ni-br sites with in-phase occupancy of adjacent Ni-br rows [Fig. 1(b)]; (II) Ni₃Al ordering but with out-of-phase occupancy of adjacent Ni-br rows (anti-phase AP); (III) perfect Ni₃Al ordering but shifted with Ni on all Ni-br and in-phase alternating Ni and Al on Al-br rows (anti-site AS); (IV) phase-separation into regions of equal areas with perfect NiAl ordering (with Ni on all Al-br and Al on all Ni-br) and with a dense Ni overlayer; (V) phase-separation into regions with a dense Ni overlayer and with dense Al overlayer with areas in the ratio 3:1 for Ni:Al.

Ni₃Al ordering (I) or (II) is preferred over 2D phase-

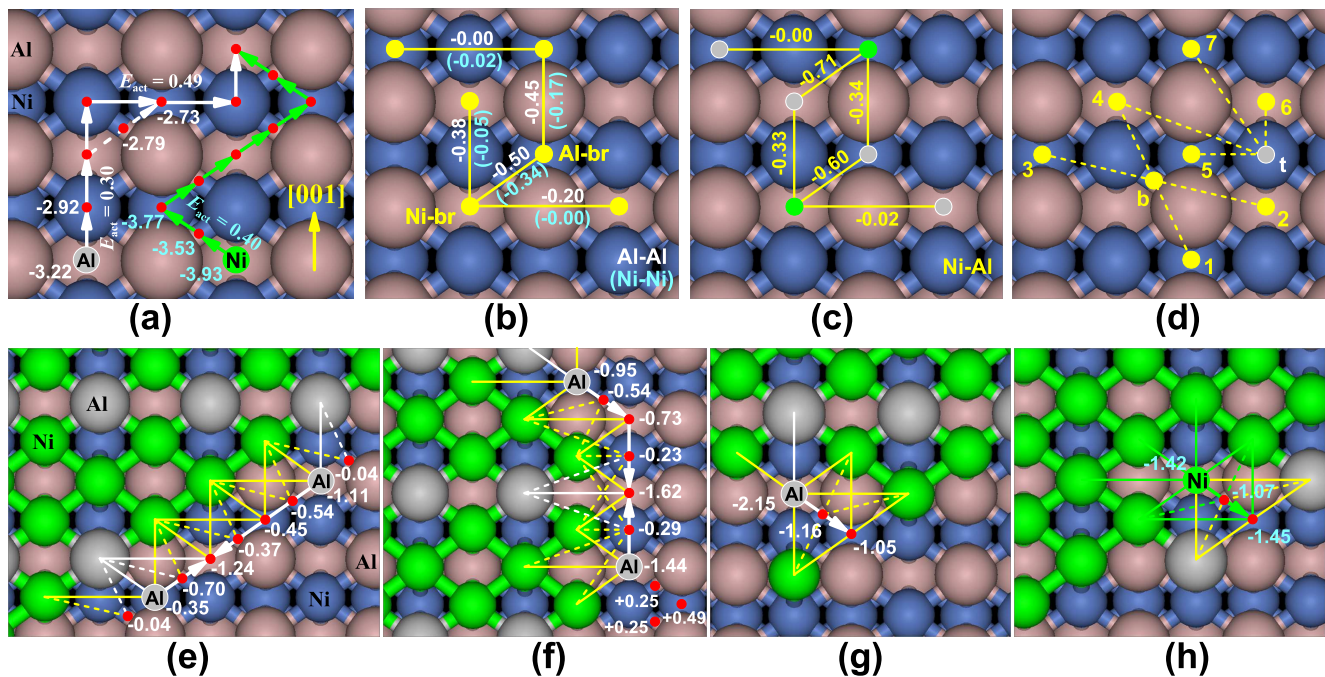


FIG. 2. (a) Adsorption energies in eV and diffusion paths for Ni and Al on NiAl(110); (b,c) pair interactions (attraction < 0) with atoms at Ni-br or Al-br sites; (b) Unconventional pair interactions with one atom at a “b” or “t” TS and one at Ni-br or Al-br; (e-f) Al diffusion along diagonal (e) and [001] (f) edges of a Ni₃Al island finding the “correct” site; (g) Al diffusion at a $[\bar{1}10]$ edge disrupting NiAl ordering. (h) Extraction of Ni aided by peripheral Al. In (e-h): site energies given relative to a Ni-br terrace site are impacted by standard (unconventional) interactions shown as thin solid (dashed) lines.

TABLE II. Pair and DFT energies in eV for various adlayers.

	I. Ni ₃ Al	II. AP	III. AS	IV. NiAl+2Ni	V. 3Ni+Al
Pair	-20.13	-19.97	-18.92	-19.90	-18.44
DFT	-19.27	-19.24	-18.77	-19.14	-17.80

separation into NiAl and Ni regions (IV). Why? This reflects a preference for alternating ordering versus 1D phase-separation of Ni and Al within each Ni-br row (since the nearest-neighbor (NN) attraction for Ni-Al pairs in Ni-rows of 0.33 eV is stronger than the average NN attraction for Ni-Ni and Al-Al pairs). Preference for perfect Ni₃Al ordering (I) versus anti-phase ordering (II) derives from a strong NN attraction of 0.20 eV between Al-Al pairs in adjacent Ni-br rows far exceeding NN attractions between other pairs of species. We find that $E_{3\text{Ni}+\text{Al}}^{(\text{I})} < E_{3\text{Ni}+\text{Al}}^{(\text{II})} < E_{3\text{Ni}+\text{Al}}^{(\text{IV})} < E_{3\text{Ni}+\text{Al}}^{(\text{III})} < E_{3\text{Ni}+\text{Al}}^{(\text{V})}$, demonstrating that perfect Ni₃Al ordering is most favorable. This preference is consistent with that from direct DFT analysis for complete adlayers. See Table II.

We can also determine the distorted octagonal equilibrium shapes of perfect Ni₃Al alloy islands. Our analysis assumes that $[\bar{1}10]$, [001], and “diagonal” steps, with lengths L_x , L_y , and L_d , respectively, are dominant. (“Diagonal” steps are aligned with the diagonals of the rectangular NiAl(110) unit cell.) Evaluation for our model of step energies, and incorporation into a Wulff construction

yields $L_d : L_x : L_y = 1.19 : 1.39 : 1$.

Kinetics of simultaneous and sequential codeposition. The most efficient pathway for formation of the thermodynamically preferred Ni₃Al overlayer nanostructures should be *simultaneous codeposition* of Ni and Al in a 3:1 ratio. KMC simulation reveals very irregular islands with poor alloy ordering at 300 K. At 400 K, there are local regions of NiAl ordering and of pure Ni, but little Ni₃Al ordering. Significant perfect in-phase Ni₃Al ordering occurs by 500 K, but islands contain local regions of NiAl ordering. “Excess Ni in these Ni₃Al + NiAl islands (overall 3:1 Ni:Al) results in predominantly Ni island edges, as incorporating Al into the interior lowers the island energy. By 600 K, one has primarily perfect Ni₃Al order, but still some regions of NiAl order and Ni-rich edges (not shown). Shapes of smaller islands at higher T are compact, but irregular non-equilibrium growth shapes develop for larger islands. See Fig. 3.

Our model provides detailed insight into the kinetics of Ni₃Al ordering. Given strong Ni-Al attraction for diagonally neighboring Ni-br and Al-br sites, Al at island edges can be trapped in the “wrong” sites. Indeed, Figs. 2(e) and 2(f) show the presence of such trap sites (with energies far below the terrace Ni-br site) on diagonal and [001] edges of alloy islands. The barrier for Al to migrate to the “correct” site for Ni₃Al order on the [001] edge is around 1.15 eV, so the process is active at 500 K with rate $\sim 25/\text{s}$, but not at 400 K or lower T . Note that different

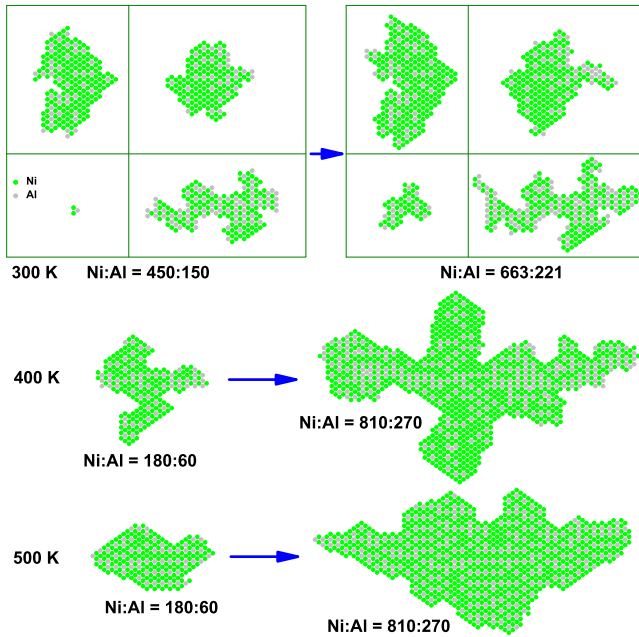


FIG. 3. KMC simulation of 2D island growth for simultaneous codeposition with 3:1 Ni:Al. Individual small islands at 300 K show composition fluctuations. Flux: 0.003 ML/s.

diffusion paths operate on different step edges necessitating inclusion of all such paths in our model. Fig. 2(g) shows an Al atom at the $[\bar{1}10]$ edge in a trap site corresponding to NiAl order. The barrier to escape such a site aided by two suitably-located nearby Ni is 1.10 eV, but higher at 1.37 (1.95) eV for one (zero) nearby Ni. This explains why NiAl order persists even at 500 K.

Island growth shapes reflect edge diffusion kinetics. Diffusion of Ni along step edges is fairly facile (effective barrier 0.71 eV along diagonal edges and somewhat higher for other orientations). This process is active above 300 K, partly quenching growth shape instability and aiding formation of locally compact islands. However, Al edge diffusion is slower [see Figs. 2(e)-2(g)], producing irregular larger islands even at 500 K.

Note that perfect Ni_3Al domains are two-fold degenerate. Deposition creates roughly equal populations of these domains (no long-range order), even within single large islands above ~ 500 K. Thus, superlattice diffraction spots for Ni_3Al order are diffuse, their inverse width reflecting domain size [19].

Sequential codeposition could provide a convenient alternative to simultaneous codeposition with better control over stoichiometry. However, can Ni_3Al order develop? Previous studies of the deposition of Al then Ni revealed the formation of a robust Al core resistant to intermixing with Ni forming a surrounding ring [15]. The barrier for extraction of Al from the core even aided by two peripheral Ni is high, around 1.7 eV for prominent [001] edges. Thus, here we consider only deposition of Ni then Al. In this case, the Ni core is vulnerable to disruption

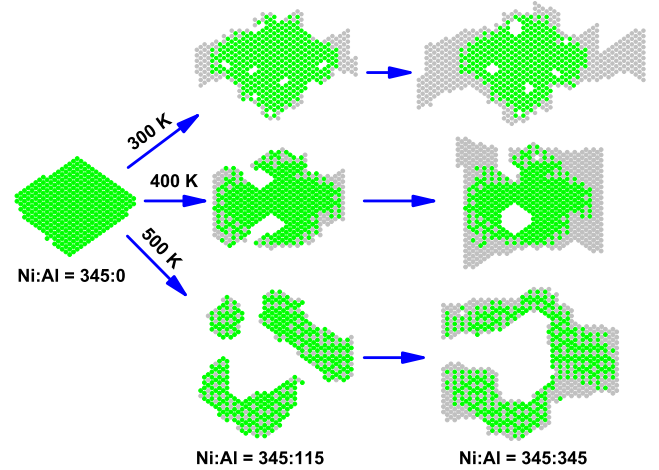


FIG. 4. KMC simulation of 2D island growth for sequential codeposition of Ni first then Al. Flux: 0.003 ML/s.

due to extraction of Ni aided by Al aggregation at the periphery. Fig. 2(h) reveals a Ni extraction barrier of only 0.35 eV aided by two Al. The Al atom below the extracted Ni can then readily take its place hopping over the Ni-top site with barrier 0.71 eV. Note that extraction aided by a single Al is still facile with barrier 0.66 eV. KMC simulation results shown in Fig. 4 indicate that 300 K, there is some disruption of the Ni core but negligible intermixing. But at 400 K, there is some intermixing at the Ni core-Al ring interface with limited NiAl and Ni_3Al ordering. By 500 K, there is complete intermixing and significant alloy ordering. For 1:3 Al:Ni compositions, there is a significant tendency for Ni_3Al ordering. With more extensive Al deposition and 1:1 Al:Ni compositions, NiAl ordering is more prominent. Interestingly, the Ni core can be completely disrupted and fragmented by aggregating Al at 500 K or above.

In summary, either simultaneous or sequential codeposition provides an effective pathway to form a novel Ni_3Al surface structure on NiAl(110) at low T . Contrasting previous codeposition protocols for alloy formation in thin films, we exert finer atomic-layer control and elucidate kinetics with realistic atomistic-level modeling.

This work was supported by NSF Grant CHE-1111500. Ames Laboratory is operated for the USDOE by ISU under Contract No. DE-AC02-07CH11358.

* Electronic mail: yong@ameslab.gov

- [1] V. K. Sikka *et al.*, *Intermetallics* **8**, 1329 (2000).
- [2] S. B. Mishra *et al.*, *Mater. Lett.* **59**, 3694 (2005).
- [3] S. Saadi *et al.*, *Surf. Sci.* **605**, 582 (2011).
- [4] A. T. Hanbicki *et al.*, *Surf. Sci.* **331**, 811 (1995).
- [5] M. Schmid *et al.*, *Phys. Rev. Lett.* **97**, 046101 (2006).
- [6] E. Vesselli *et al.*, *Phys. Rev. Lett.* **105**, 046102 (2010).
- [7] M. Kulawik, N. Nilius, and H.-J. Freund, *Phys. Rev. Lett.* **96**, 036103 (2006).

- [8] M. Chen and D. W. Goodman, *Chem. Phys. Sol. Surf.* **12**, 201 (2007).
- [9] A. Lehnert *et al.*, *Surf. Sci.* **600**, 1804 (2006).
- [10] G. Prévot *et al.*, *Surf. Sci.* **604**, 770 (2010).
- [11] M. Petrantoni *et al.*, *J. Vac. Sci. Tech. A* **28**, L15 (2010).
- [12] J.-K. Ho *et al.*, *J. Vac. Sci. Tech. A* **13**, 2170 (1995).
- [13] A. J. Gavens *et al.*, *J. Appl. Phys.* **87**, 1255 (2000).
- [14] M. L. Anderson *et al.*, *Phys. Rev. Lett.* **98**, 096106 (2007).
- [15] A. K. Schmid *et al.*, *Science* **290**, 1561 (2000).
- [16] E. Vesselli *et al.*, *J. Phys. Cond. Mat.* **20**, 195223 (2008).
- [17] T. Duguet *et al.*, *Proc. Nat. Acad. Sci.* **108**, 989 (2011).
- [18] Y. Han *et al.*, *Phys. Rev. B* **84**, 113414 (2011).
- [19] J. W. Evans, P. A. Thiel, and M. C. Bartelt, *Surf. Sci. Rep.* **61**, 1 (2006).
- [20] Y. Han *et al.*, *J. Chem. Phys.* **135**, 084706 (2011).